HAL
open science

# Luminescence-Driven Electronic Structure Determination in a Textbook Dimeric Dy(III)-based Single Molecule Magnet

Djamila Guettas, Frédéric Gendron, Guglielmo Fernandez Garcia, François Riobé, Thierry Roisnel, Olivier Maury, Guillaume Pilet, Olivier Cador, Boris Le Guennic

## To cite this version:

Djamila Guettas, Frédéric Gendron, Guglielmo Fernandez Garcia, François Riobé, Thierry Roisnel, et al.. Luminescence-Driven Electronic Structure Determination in a Textbook Dimeric Dy(III)-based Single Molecule Magnet. Chemistry - A European Journal, 2020, 26 (19), pp.4389-4395. 10.1002/chem.201905493 . hal-02472163

## HAL Id: hal-02472163

## https://univ-rennes.hal.science/hal-02472163

Submitted on 17 Feb 2020

**HAL** is a multi-disciplinary open access archive for the deposit and dissemination of scientific research documents, whether they are published or not. The documents may come from teaching and research institutions in France or abroad, or from public or private research centers.

L'archive ouverte pluridisciplinaire **HAL**, est destinée au dépôt et à la diffusion de documents scientifiques de niveau recherche, publiés ou non, émanant des établissements d'enseignement et de recherche français ou étrangers, des laboratoires publics ou privés.

# Luminescence-Driven Electronic Structure Determination in a Textbook Dimeric Dy(III)-based Single Molecule Magnet

Djamila Guettas,[a] Frédéric Gendron,[b] Guglielmo Fernandez Garcia,[b,c] François Riobé,[d] Thierry Roisnel,[b] Olivier Maury,*[d] Guillaume Pilet,*[a] Olivier Cador,*[b] Boris Le Guennic,*[b]

**Abstract:** A textbook dysprosium dinuclear complex based on acethylacetonate ligands, $[Dy_2(acac)_4(\mu_2\text{-acac})_2(H_2O)_2]$ has been synthesized and fully characterized. This simple dimeric lanthanide complex shows well-resolved solid-state luminescence and behaves as a Single Molecule Magnet under zero DC field. A seminal crystal field approach is used to marry both magnetism and luminescence in the frame of an energetic picture.

## Introduction

Since the discovery of mononuclear based Single-Molecule magnets (SMMs),[1] lanthanide ions are the cornerstone of a new generation of molecular magnets.[2–6] In particular, these molecular objects are promising for applications as single component in nanospin manipulation.[7–9] While their performances stagnated for a decade around 14 K[10] large step forward recently occurs with organometallic mononuclear based compounds that store magnetic information around liquid nitrogen temperature.[11–13] These magnets are constituted of Ln(III) ions which possess large magnetic moment associated with a huge magnetic anisotropy. In parallel, lanthanides are well known to emit lights from UV to NIR range with characteristic emission bands[14]. This luminescence arises from formally Laporte forbidden f-f transitions with long lifetime and very weak absorption coefficient. To overcome this lock suitable ligands are used as antennae to sensitize the emission.[15–17]

[a] Dr. D. Guettas, Dr. G. Pilet
Laboratoire des Multimatériaux et Interfaces (LMI), UMR 5615 CNRS-Université Claude Bernard Lyon 1, bâtiment Chevreul, Avenue du 11 novembre 1918, 69622 Villeurbanne cedex (France)
E-mail: guillaume.pilet@univ-lyon1.fr

[b] Dr. G. Fernandez Garcia, Pr. O. Cador, Dr. T. Roisnel, Dr. B. Le Guennic
Univ Rennes, CNRS, ISCR (Institut des Sciences Chimiques de Rennes) - UMR 6226, 35000 Rennes (France)
E-mail: boris.leguennic@univ-rennes1.fr

[c] Dr. G. Fernandez Garcia
Dipartimento di Chimica "U.Schiff" and UdR INSTM Università degli Studi di Firenze, Via della Lastruccia 3-13, 50019 Sesto Fiorentino (Italy)

[d] Dr. O. Maury, Dr. F. Riobé
Univ Lyon, ENS Lyon, CNRS UMR 5182, Laboratoire de Chimie, 46 allée d'Italie, 69364 Lyon cedex 07 (France)
E-mail : olivier.maury@ens-lyon.fr

Supporting information for this article is given via a link at the end of the document

In a pioneering paper, van Vleck pointed out that crystal field splitting (CFS) is at the origin of both magnetism and luminescence and consequently both properties are strongly correlated.[18] Indeed, luminescence and magnetism both originate from crystal field of 4f orbitals. Some of us and other groups contributed to the revival of this old idea and in the beginning of the 2010's established correlation between magnetic and luminescence on Dy(III)- but also Yb(III)-based SMMs.[19–26] These results triggered a new interest into high-resolution luminescence measurements in order to experimentally establish the complete diagram of luminescent SMMs. Although classical, such determination can be quite tricky because of the presence of "extra-transitions" in the luminescence spectra assigned sometimes too rapidly to "hot bands" or vibronic transitions[3,27,28] (see also Ref.[29–31] for Dy(III)).

On the magnetic aspects, one of the major issue with mononuclear SMMs is the presence of sizable Quantum Tunnelling of Magnetization (QTM) at low temperature which prevents the opening of the magnetic hysteresis loop.[5,32,33] This problem can be solved in minimizing internal field through either dilution in a diamagnetic matrix or cancellation of the nuclear spin via isotopic enrichment.[7,34–37] Another efficient possibility is to couple the magnetic centres (superexchange and/or dipolar interactions) within a polynuclear edifice.[38–46]

Recently, some of us developed synthetic strategies based on diketone moieties, which are well known ligands to coordinate lanthanide ions. Although these pincers can present several coordination modes, it is possible by controlling the synthesis parameters (pH, temperature, time…) to isolate *à la carte* polynuclear complexes[47–50]. Herein, we report a textbook dysprosium dinuclear complex based on acetylacetonate ligand (the simplest diketonate). The goal of this work is to use seminal crystal field approach to marry magnetism and luminescence in the frame of an energetic picture.

## Results and Discussion

### Synthesis and crystal structure

Acetylacetone (Hacac, 1eq.) and $Et_3N$ (1.5 eq.) were added dropwise to a methanolic solution of $DyCl_3{\cdot}6H_2O$ (0.5 eq.). After 10 min. of stirring, the clear colourless mixture was filtrated and the filtrate was left undisturbed at room temperature. After two days of slow evaporation of the solvent, single-crystals of $[Dy_2(acac)_4(\mu_2\text{-acac})_2(H_2O)_2]$ **Dy₂**, suitable for single-crystal X-ray

Accepted Manuscript

analysis, were obtained (43% yield) (Table SI-1). The centrosymmetrical dimer is constituted of six deprotonated acac$^-$ ligands, two coordinated water molecules and two Dy(III) cations. This latter is located in a {$O_8$} environment where five oxygen atoms (O31, O37, O27, O17, O11) belong to three terminal acac$^-$ ligands, one oxygen atom (O1) to a coordinated water molecule. The bridging acac$^-$ ligands (O27, O21) binding in a μ,κ$_1$:κ$_2$-acac-O,O′ mode complete the coordination sphere of the lanthanide cation (Figure 1). The oxygen atom O21 bridges the two Dy(III) ions with intermolecular Dy···Dy distances equal to 4.0363(4) Å (Table SI-2). The SHAPE analysis [20] reveals that the Dy(III) ions seat in an almost perfect square antiprism environment (Table SI-3). Dy-O bond length involving water molecule and terminal acac$^-$ ligands (2.361(3) Å and ~2.332 Å) are slightly shorter than those for oxygen atoms involved in the Ln-O-Ln symmetrical double bridge (~2.465 Å). All these bonds lengths are in good agreement with those usually observed for Ln(III) dimers with fully oxygenated coordination sphere[51]. Intramolecular hydrogen bond involves coordinated water molecule and oxygen atom of one acac$^-$ with O···O distance equal to 2.646 Å. Hydrogen bond (intermolecular) involves the other hydrogen atom of the water molecule and oxygen atom of one acac$^-$ of neighbouring molecule. These intermolecular hydrogen bonds create chains of dimers along *a*-axis. The shortest inter-dimer Dy…Dy distance is equal to 6.0816(7) Å. Sample purity was checked by powder X-ray diffraction experiment comparing experimental diagram to theoretical one obtained from crystal structure (Figure SI-1).

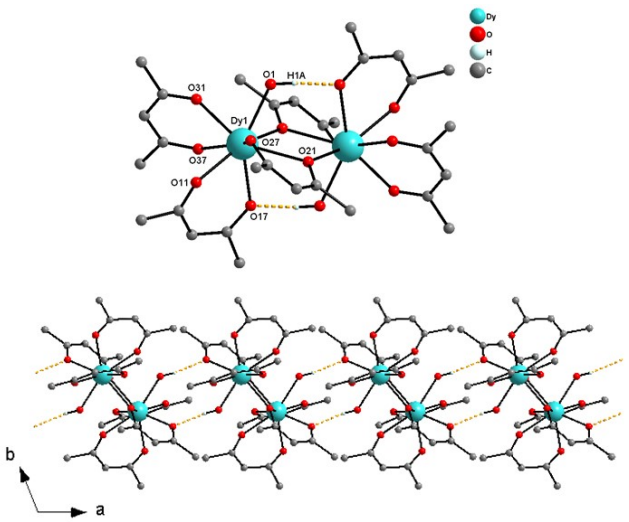


**Figure 1.** (top) view of **Dy$_2$** dimer with major labels and intra-hydrogen bonds (orange dashed lines); (bottom) chains of **[Dy$_2$]** dimers running along the *a*-axis of the unit-cell with inter-hydrogen bonds. For clarity, hydrogen atoms not involved in hydrogen bonds have been omitted.

## Photophysical properties

Photophysical measurements were performed on a polycrystalline sample at room and low temperatures. Upon direct excitation of the lanthanide at 363 nm, classical luminescence of Dy(III) was observed with three main sharp bands localized in the visible at 482, 576 and 662 nm corresponding to 4*f*-4*f* transitions from the $^4F_{9/2}$ excited level to the $^6H_{15/2}$, $^6H_{13/2}$ and $^6H_{11/2}$ levels, respectively (Figure 2).

A zoom of high-resolution excitation and emission spectra were obtained at 77 K revealing the sub-level splitting (crystal field splitting) of $^4F_{9/2}$ and $^6H_{15/2}$ levels, respectively (Figure 2). The excitation spectrum clearly shows five main transitions (474.8, 472.8, 471.2, 468.4 and 466.8 nm) as expected for the $^4F_{9/2}$ level giving a clear and complete spectroscopic picture of the excited state. The analysis of the ground state sub-levels splitting is more complicated with overlap of the expected eight transitions. However, the band at 474.6 nm matches perfectly well with the lowest energy transition of the excitation spectrum and therefore can be unambiguously assigned to "zero-phonon" transition (transition between the lowest $m_J$ sub-levels). It is worth noting that emission generally occurs from the lowest energy excited state and particularly from its lowest crystal field sub-levels. However, due to thermal effects, excited $m_J$ states can be populated according to a classical Boltzmann distribution that can be calculated from the splitting of the excited state (Figure 3). The details of the calculations are given in SI. They indicate that all $m_J$ excited states are populated at room temperature and will all contribute to the emission spectrum via the so-called "hot bands" (5×8 = 40 expected transitions). Decreasing the temperature will depopulate the $m_J$ excited states and considerably simplify the emission spectrum. Therefore, variable temperature emission spectra were recorded between 200 and 7 K (Figure 3) and the excited $m_J$ states population is compiled in Table SI-5.

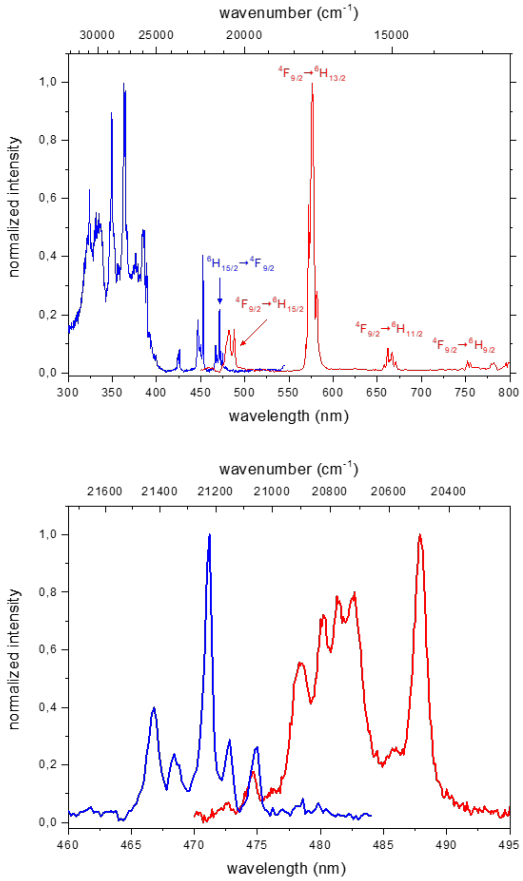


**Figure 2.** (top) Solid state excitation (blue) and emission (red) spectra of **Dy$_2$** recorded at 77 K. (bottom) High resolution spectra of the 460-495 nm range corresponding to the $^4F_{9/2}\rightarrow{}^6H_{15/2}$ emission bands.

Accepted Manuscript

At 200 K, the theoretical Boltzmann distribution indicated that all the $m_J$ excited states are populated with three major contributions $N_0$, $N_1$ and $N_2$ (Table SI-5). Their contributions to the emission spectrum are clearly evidenced by the presence of two transitions (noted $h_1$ and $h_2$, Figure 3) at higher energy compared to the zero phonon one (noted 0 on Figure 3), and match perfectly with the excitation bands. On cooling, the hot band $h_2$ disappears at higher temperature (75 K) than $h_1$ (25 K). These observations are in good accordance with the calculated Boltzmann distribution (Table SI-5). Therefore, below 15 K, no hot bands are visible anymore. Considering the unresolved two contributions merged in the rounded band at 477.8 nm, the emission spectrum is unambiguously composed of seven clear transitions. The additional shoulder observed at 473.4 nm leads to the complete eight-level energy diagram expected for the $^6H_{15/2}$ level in relatively low symmetry environment (474.2, 477.6, 478.0, 479.8, 481.0, 482.2, 483.4(s) and 487.4 nm). The last small band observed at lower energy ($v_1$) is assigned to a vibronic contribution. Overall, this study enables us to determine the complete CFS energy diagram of the ground level $^6H_{15/2}$ (0, 150, 168, 246, 298, 354, 384, 571 cm$^{-1}$) and particularly the Δ value, corresponding to the energy gap between the two first $m_J$ states of the $^6H_{15/2}$ level of 150 cm$^{-1}$.

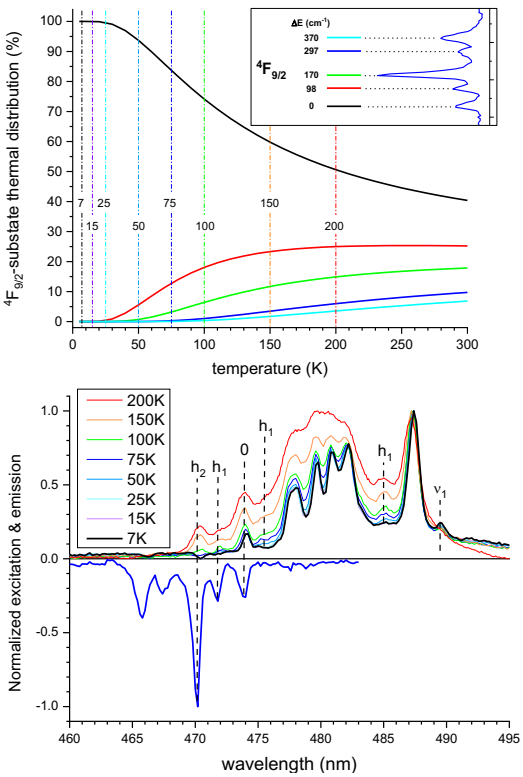


Figure 3. (top) theoretical Boltzmann population of the $m_J$ sub-levels of the $^4F_{9/2}$ excited state. In inset is represented the energy diagram of the $^4F_{9/2}$ excited state obtained from the solid-state excitation spectrum measured at 77 K; (bottom) variation of the solid-state emission with temperature, in negative value (blue) is represented the excitation spectrum at 77 K.

## Crystal-Field and Static Magnetic Properties

Taking the advantage of the previous photo-physical analysis and of the almost perfect $D_{4d}$ coordination sphere around the Dy(III) ion, an attempt at determining the electronic structure and the magnetic properties of **$Dy_2$** was performed by using crystal-field (CF) theory. Indeed, the CF Hamiltonian of a *4f* ion placed in a $D_{4d}$ environment can be written as follows:

$$\hat{H}^{CF} = \alpha_J[B_2^0\tilde{O}_2^0(J)] + \beta_J[B_4^0\tilde{O}_4^0(J)] + \gamma_J[B_6^0\tilde{O}_6^0(J)] \quad \text{(Eq 1.)}$$

where the $\alpha_J$, $\beta_J$ and $\gamma_J$ are parameters obtained using the Wigner-Eckard theorem and depend on the considered J-manifold (here J = 15/2 and $\alpha_J$, $\beta_J$ and $\gamma_J$ coefficients are equal to -2/315, -8/135135 and 4/3864861, respectively), the $\tilde{O}_k^q(J)$ are the Stevens operators, and the $B_k^q$ terms are the CF parameters. Assuming that the ground multiplet $^6H_{15/2}$ is well separated from the other excited multiplets, the matrix elements $\langle J, M_J|\tilde{O}_k^q|J, M_J'\rangle$ can be then simply determined by using the values originally tabulated by Stevens.[52] The 16-fold degeneracy of the $^6H_{15/2}$ multiplet is released, but without any admixture between the $m_J$ states.

The CF parameters were therefore determined with a least squares procedure by fitting the energies determined from the analyses of the emission spectra. The resulting determined energies, calculated with $B_2^0$ = -60 cm$^{-1}$, $B_4^0$ = -118 cm$^{-1}$ and $B_6^0$ = +150 cm$^{-1}$, are given in Table 1. A relatively good agreement was obtained between the fitted and experimentally observed energies (root mean square deviation of the fitted energies equal to 19.61). The fitted CF parameters lead to a ground state (GS) corresponding to $m_J$ = +/-13/2, whereas the highest $m_J$ state (+/-15/2) is found at 562 cm$^{-1}$ above the GS.

**Table 1.** Relative energies (in cm$^{-1}$), $m_J$ wave-functions

| | ΔE Exp | ΔE CF | \|15/2, $m_J$> |
|---|---|---|---|
| GS | 0 | 0 | 13/2 |
| ES1 | 150 | 100 | 11/2 |
| ES2 | 168 | 160 | 1/2 |
| ES3 | 246 | 245 | 3/2 |
| ES4 | 298 | 308 | 9/2 |
| ES5 | 354 | 356 | 5/2 |
| ES6 | 384 | 401 | 7/2 |
| ES7 | 571 | 562 | 15/2 |

In order to confirm this electronic structure, static magnetic susceptibility measurements were performed on polycrystalline sample. The $\chi_M T$ vs T curve is shown in Figure 4. The room temperature value of the $\chi_M T$ is 26.7 cm$^3$ K mol$^{-1}$, which is very close to the expected value (28.34 cm$^3$ K mol$^{-1}$) for two isolated Dy(III) ions. $\chi_M T$ decreases continuously on cooling because of the combine effect of the thermal depopulation of the CF states of the $^6H_{15/2}$ level and the interaction between magnetic centres within the dimer (Figure 4). Meanwhile, magnetization at 2 K does not saturate at high field and does not reach 5.00 Nβ per Dy(III) (inset, Figure 4) like it would be expected for the stabilization of the Ising components $M_J$ = +/-15/2 of the GS multiplet (9.3 instead of 10.0 Nβ at 50 kOe). The $\chi_M T$ *vs* T curve was then fitted over the whole temperature range by using the following total Hamiltonian:

$$\hat{H} = \hat{H}^{CF} + \beta g_J(\hat{J}_1 + \hat{J}_2)\cdot\vec{H} + \hat{J}_1\cdot D\cdot\hat{J}_2 \quad \text{(Eq 2.)}$$

where the first and second part of the Hamiltonian correspond to the CF and Zeeman interactions, respectively, acting on the full J = 15/2 manifold, whereas the third part of the Hamiltonian corresponds to the magnetic interaction between the two Dy(III) centres. The experimental curve was fitted with only one free

Accepted Manuscript

parameter: the interaction D. CF parameters $B_2^0$, $B_4^0$ and $B_6^0$ are set and fixed from spectroscopy (*vide supra*). The fitted $\chi_M T$ vs. T curve is represented on Figure 4. It properly reproduces the experimental data with D=-8.31×10$^{-3}$ cm$^{-1}$ and an agreement factor $R^2$=1.57×10$^{-4}$. The M vs. H curve at 2 K is then simulated with the same set of parameters and matches well the experimental curve.

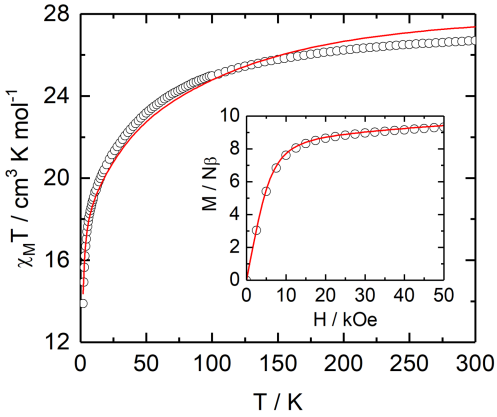


**Figure 4.** Temperature dependence of $\chi_M T$ of **Dy₂**. Inset: field dependence of the magnetization for **Dy₂** measured at 2 K. Red lines are best fitted curves.

Single-crystal magnetometry performed at very low temperature provides a unique tool to probe (*i*) the magnetic anisotropy of the ground state and (*ii*) the orientation of the principal magnetic axes, always in the ground state. However, such technique is subject to crystallographic restrictions. Indeed, if the interaction between magnetic centres is weak with respect to thermal energy, the quantitative analysis is restricted to one crystallographic site. Furthermore, since the measurement is averaged over all the magnetic moments in a single-crystal, only one orientation is tolerated which restricts the application domain to P1 and P-1 space groups, as is for the present **Dy₂** structure. In the effective spin frame, each Dy(III) ion can be viewed as a spin ½ with the principal g-values $g_{xx}$ = 5.03, $g_{yy}$ = 5.59 and $g_{zz}$ = 12.98 (Figure SI-2 and SI-3). Clearly, the magnetic anisotropy is not purely axial and the Dy(III) magnetic moment cannot be considered as Ising. The error induced on susceptibility measurements by the application of a moderate field of 1 kOe for a single-crystal measurement, which might induce saturation effect as well as decoupling of the two magnetic moments, is not significant (Figure SI-3) with less than 2% difference between low filed (13.88 cm$^3$ K mol$^{-1}$ at 200 Oe) and 1 kOe (13.66 cm$^3$ K mol$^{-1}$) at 2 K. The orientation of the g-tensor is given on Figure 5. The most magnetic axis is clearly oriented along the two *acac*$^-$ moieties and is perpendicular to Dy-O(water) direction. The determination of the orientation of the magnetic axes give the possibility to calculate the dipolar contribution, $J_{Dip}$ to the interaction between the two Dy(III) ions. $J_{Dip}$ is calculated equal to -0.008 cm$^{-1}$ and matches almost perfectly with the estimated D value from $\chi_M T$ vs. T curve. This suggests that the interaction is entirely of dipolar origin.

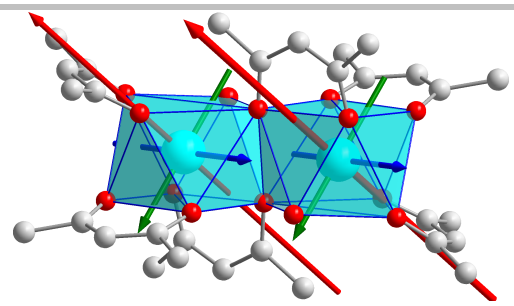

**Figure 5.** Orientation of the principal axes $g_{xx}$ (green), $g_{yy}$ (blue) and $g_{zz}$ (red) with respect to the molecule orientation in **Dy₂**.

## Dynamic magnetic susceptibility

Both in-phase, $\chi_M'$, and out-of-phase, $\chi_M''$, components of the ac susceptibility show frequency dependence below 6 K with the frequency of the ac magnetic field (Figure 6) in the absence of an external dc magnetic field. These are characteristic of the presence of slow relaxation of the magnetic moment of the dimer and the signature of a SMM. The ac data can be quantitatively analysed with an extended Debye model (see SI, Table SI-6 and Figure SI-4). In this frame, the distribution of the relaxation time is relatively narrow with the empiric parameter $\alpha$ comprised between 0.06 and 0.12. In addition, the non-relaxing fraction of the magnetic moment, defined as the percentage between the high and low frequency limits of the susceptibility is relatively constant close to 13% (Table SI-6). This attests that most of the magnetic moment relaxes at single frequency. The temperature dependence of the relaxation time is represented on Figure 7. It can be analysed with the following equation:

$$\tau^{-1} = \underbrace{\tau_0^{-1}\exp\left(\frac{\Delta}{T}\right)}_{Orbach} + \underbrace{CT^n}_{Raman} + \underbrace{\frac{B_1}{1+B_2H^2}}_{QTM} + \underbrace{ATH^m}_{Direct} \quad \text{(Eq 3.)}$$

Which features four different processes that depend or not on temperature and external dc magnetic field. In our case, the external magnetic field is not involved so the direct process is not considered and the QTM becomes temperature independent. The Orbach process involves an energy barrier that can be considered as the gap between the ground and the first excited state which is set at 150 cm$^{-1}$. Compared to experimental data the Orbach process, even in considering extremely fast and very unrealistic intrinsic relaxation time $\tau_0$ = 10$^{-20}$ s, is much too slow to be considered (vertical green line on Figure 7) with $\Delta$ = 216 K (150 cm$^{-1}$). In this frame, the temperature dependence of the relaxation time is fitted with only Raman and QTM processes (Figure 7). The best fitted curve is obtained with C = 3.34 s$^{-1}$ K$^{-n}$, n = 5.044 and $B_1^{-1}$ = $\tau_{QTM}$ = 4.66×10$^{-4}$ s (Figure 7).

Accepted Manuscript

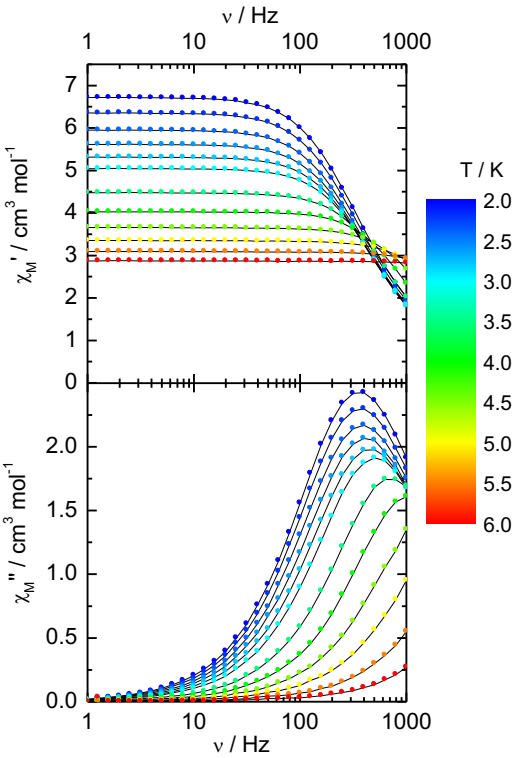


**Figure 6.** Frequency dependence of the in-phase, $\chi_M'$, and out-of-phase, $\chi_M''$, components of the *ac* susceptibility measured in zero external *dc* field for **$Dy_2$**.

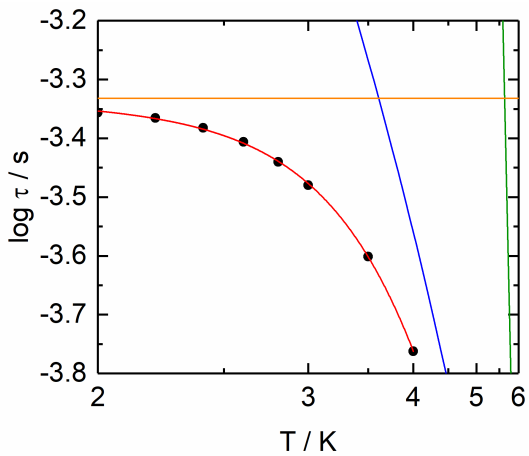


**Figure 7.** Temperature dependence of the relaxation time of the magnetic moment of **$Dy_2$** (black dots) with the best fitted curve with Raman+QTM processes (red line). The Orbach process with $\Delta$=150 cm$^{-1}$ is represented as green line. The separated contributions from Raman (blue line) and QTM (orange line) are also represented.

## Conclusion

This paper focused on a textbook example of Dy(III) dimer behaving as a luminescent Single-Molecule Magnet in zero external dc field. Boltzmann statistics applied to solid-state variable temperature luminescence coupled with excitation spectroscopy at liquid nitrogen temperature allows to unambiguously extract the low-lying ($^6H_{15/2}$ manifold) energy diagram. Seminal Stevens theory applied on this energy picture provides crystal field parameters that can be injected in the simulation of the magnetic susceptibility with only the magnetic interaction between Dy(III) ions as a free parameter. These investigations emphasize that optical spectroscopies and magnetism work hand in hand to give a complete view on the ground state multiplet splitting. Standing on this experimental evidence we demonstrate that Orbach process (relaxation through the first excited state) is not involved in the dynamics of the magnetization.

## Experimental Section

**Single-crystal X-ray diffraction** was carried out by using a Gemini diffractometer and the related software. An absorption correction based on the crystal faces was applied to the data sets (analytical). The structure was solved by direct methods using the SHELXT program[53], and then refined with full-matrix least-square methods based on F2 (SHELXL-97)[54]. All non-hydrogen atoms were refined with anisotropic atomic displacement parameters. Except hydrogen atoms of water molecule that were introduced in the structural model through Fourier difference maps analysis, H atoms were finally included in their calculated positions. All atomic displacement parameters for non-hydrogen atoms were refined with anisotropic terms. CCDC-1970193 contains the supplementary crystallographic data for this paper. These data can be obtained free of charge from the Cambridge Crystallographic Data Centre via www.ccdc.cam.ac.uk/data_request/cif.

**Magnetic measurements.** Magnetic susceptibility data (2-300 K) were collected on powdered polycrystalline samples on a Quantum Design MPMS-XL SQUID magnetometer under an applied magnetic field of 0.02 T below 20 K, 0.2 T between 20 and 80 K and finally 1 T above 80 K using a pelletized sample in Teflon tape to prevent orientation within the magnetic field. Alternating current (ac) measurements were performed in the 2-6 K range in zero external dc field in 1-1000 Hz range. Magnetization isotherm was collected at 2 K. All data were corrected for the contribution of the sample holder and the diamagnetism estimated from Pascal's constants.

**Photophysical measurements.** Solid state emission and excitation spectra were measured using a Horiba-JobinYvon Fluorolog-3® spectrofluorimeter, equipped with a three slit double grating excitation and emission monochromator with dispersion of 2.1 nm/mm (1 200 grooves/mm). The steady-state luminescence was excited by unpolarised light from a 450 W xenon CW lamp and detected at an angle of 90° by a Hamamatsu R928 photomultiplier tube (200-900 nm). Spectra were reference corrected for both the excitation intensity variation and the emission spectral response. Solid sample was placed in a 0.5 mm diameter quartz tube that was cool down either in a liquid nitrogen dewar (77K) or set into an Oxford Instrument cryostat (Optistat CF2) insert directly in the sample chamber of the spectrofluorimeter. The interference signals due to scattered excitation light were suppressed by a 400 nm high pass filter placed at the entry of emission monochromator. Luminescence decay plot were obtained by pulsed excitation using a FL-1040 UP xenon lamp and lifetimes were obtained by an exponential least-squares fitting using Origin®.

## Acknowledgements

D.G. is grateful to the PhD fellowship from Ecole Doctorale de Chimie belonging to Université Claude Bernard Lyon 1. Additional support was provided by the Université Claude Bernard Lyon 1,

Accepted Manuscript

ENS-Lyon and the Région Rhône-Alpes (CMIRA2015). O.M. and F.R. are grateful to ANR (REDIVALAN ANR-15-CE29-0019-02 and SCOSIMLIGHT ANR-13-BS07-0022-01) for the financial support to acquire the cryostat set-up. G.F.G. gratefully acknowledges the European Commission through the ERCAdG 267746 MolNanoMas (Project 267746) for financial support.

**Keywords:** Dysprosium • Luminescence • Single Molecule Magnet • Supramolecular chemistry • Crystal field

[1] N. Ishikawa, M. Sugita, T. Ishikawa, S. Koshihara, Y. Kaizu, *J. Am. Chem. Soc.* **2003**, *125*, 8694–8695.
[2] D. N. Woodruff, R. E. P. Winpenny, R. A. Layfield, *Chem. Rev.* **2013**, *113*, 5110–5148.
[3] F. Pointillart, O. Cador, B. Le Guennic, L. Ouahab, *Coord. Chem. Rev.* **2017**, *346*, 150–175.
[4] R. Sessoli, A. K. Powell, *Coord. Chem. Rev.* **2009**, *253*, 2328–2341.
[5] J. Tang, P. Zhang, *Lanthanide Single Molecule Magnets*, Springer, **2015**.
[6] R. A. Layfield, M. Murugesu, *Lanthanides and Actinides in Molecular Magnetism*, Wiley-VCH, Weinheim, **2015**.
[7] E. Moreno-Pineda, M. Damjanović, O. Fuhr, W. Wernsdorfer, M. Ruben, *Angew. Chem. Int. Ed.* **2017**, *56*, 9915–9919.
[8] A. Cornia, P. Seneor, *Nat. Mater.* **2017**, *16*, 505–506.
[9] S. Sanvito, *Nat. Phys.* **2010**, *6*, 562–564.
[10] J. D. Rinehart, M. Fang, W. J. Evans, J. R. Long, *J. Am. Chem. Soc.* **2011**, *133*, 14236–14239.
[11] F.-S. Guo, B. M. Day, Y.-C. Chen, M.-L. Tong, A. Mansikkamäki, R. A. Layfield, *Angew. Chem. Int. Ed.* **2017**, *56*, 11445–11449.
[12] C. A. P. Goodwin, F. Ortu, D. Reta, N. F. Chilton, D. P. Mills, *Nature* **2017**, *548*, 439–442.
[13] F.-S. Guo, B. M. Day, Y.-C. Chen, M.-L. Tong, A. Mansikkamäki, R. A. Layfield, *Science* **2018**, *362*, 1400–1403.
[14] A. de Bettencourt-Dias, *Luminescence of Lanthanide Ions in Coordination Compounds and Nanomaterials*, John Wiley & Sons, Ltd, **2014**.
[15] A. D'Aleo, F. Pointillart, L. Ouahab, C. Andraud, O. Maury, *Coord. Chem. Rev.* **2012**, *256*, 1604–1620.
[16] J.-C. G. Bünzli, C. Piguet, *Chem. Soc. Rev.* **2005**, *34*, 1048–1077.
[17] S. V. Eliseeva, J.-C. G. Bünzli, *Chem. Soc. Rev.* **2009**, *39*, 189–227.
[18] J. H. Van. Vleck, *J. Phys. Chem.* **1937**, *41*, 67–80.
[19] G. Cosquer, F. Pointillart, J. Jung, B. Le Guennic, S. Golhen, O. Cador, Y. Guyot, A. Brenier, O. Maury, L. Ouahab, *Eur. J. Inorg. Chem.* **2014**, *2014*, 69–82.
[20] F. Pointillart, B. Le Guennic, S. Golhen, O. Cador, L. Ouahab, *Chem. Commun.* **2013**, *49*, 615–617.
[21] G. Cucinotta, M. Perfetti, J. Luzon, M. Etienne, P.-E. Car, A. Caneschi, G. Calvez, K. Bernot, R. Sessoli, *Angew. Chem. Int. Ed.* **2012**, *51*, 1606–1610.
[22] M.-E. Boulon, G. Cucinotta, J. Luzon, C. Degl'Innocenti, M. Perfetti, K. Bernot, G. Calvez, A. Caneschi, R. Sessoli, *Angew. Chem. Int. Ed.* **2013**, *52*, 350–354.
[23] J. Long, R. Vallat, R. A. S. Ferreira, L. D. Carlos, F. A. A. Paz, Y. Guari, J. Larionova, *Chem. Commun.* **2012**.
[24] J. Long, *Front. Chem.* **2019**, *7*, DOI 10.3389/fchem.2019.00063.
[25] J. Long, Y. Guari, R. A. S. Ferreira, L. D. Carlos, J. Larionova, *Coord. Chem. Rev.* **2018**, *363*, 57–70.
[26] G. Brunet, R. Marin, M.-J. Monk, U. Resch-Genger, D. A. Gálico, F. A. Sigoli, E. A. Suturina, E. Hemmer, M. Murugesu, *Chem. Sci.* **2019**, *10*, 6799–6808.
[27] F. Pointillart, B. le Guennic, O. Cador, O. Maury, L. Ouahab, *Acc. Chem. Res.* **2015**, *48*, 2834–2842.
[28] J.-H. Jia, Q.-W. Li, Y.-C. Chen, J.-L. Liu, M.-L. Tong, *Coord. Chem. Rev.* **2019**, *378*, 365–381.
[29] L. Norel, L. E. Darago, B. Le Guennic, K. Chakarawet, M. I. Gonzalez, J. H. Olshansky, S. Rigaut, J. R. Long, *Angew. Chem. Int. Ed.* **2018**, *57*, 1933–1938.
[30] F. Guégan, F. Riobé, O. Maury, J. Jung, B. L. Guennic, C. Morell, D. Luneau, *Inorg. Chem. Front.* **2018**, *5*, 1346–1353.
[31] Y. Bi, C. Chen, Y.-F. Zhao, Y.-Q. Zhang, S.-D. Jiang, B.-W. Wang, J.-B. Han, J.-L. Sun, Z.-Q. Bian, Z.-M. Wang, et al., *Chem. Sci.* **2016**, *7*, 5020–5031.
[32] T. T. da Cunha, J. Jung, M.-E. Boulon, G. Campo, F. Pointillart, C. L. M. Pereira, B. Le Guennic, O. Cador, K. Bernot, F. Pineider, et al., *J. Am. Chem. Soc.* **2013**, *135*, 16332–16335.
[33] F.-S. Guo, A. K. Bar, R. A. Layfield, *Chem. Rev.* **2019**, *119*, 8479–8505.
[34] F. Pointillart, K. Bernot, S. Golhen, B. Le Guennic, T. Guizouarn, L. Ouahab, O. Cador, *Angew. Chem. Int. Ed.* **2015**, *54*, 1504–1507.
[35] J. F. Gonzalez, F. Pointillart, O. Cador, *Inorg. Chem. Front.* **2019**, *6*, 1081–1086.
[36] E. Moreno-Pineda, G. Taran, W. Wernsdorfer, M. Ruben, *Chem. Sci.* **2019**, *10*, 5138–5145.
[37] L. Tesi, Z. Salman, I. Cimatti, F. Pointillart, K. Bernot, M. Mannini, R. Sessoli, *Chem. Commun.* **2018**, *54*, 7826–7829.
[38] J. Lu, V. Montigaud, O. Cador, J. Wu, L. Zhao, X.-L. Li, M. Guo, B. Le Guennic, J. Tang, *Inorg. Chem.* **2019**, *58*, 11903–11911.
[39] P. H. Lin, T. J. Burchell, R. Clérac, M. Murugesu, *Angew. Chem. Int. Ed.* **2008**, *47*, 8848–8851.
[40] Z. Zhu, M. Guo, X.-L. Li, J. Tang, *Coord. Chem. Rev.* **2019**, *378*, 350–364.
[41] F. Pointillart, Y. Le Gal, S. Golhen, O. Cador, L. Ouahab, *Chem.- Eur. J.* **2011**, *17*, 10397–10404.
[42] F. Pointillart, S. Golhen, O. Cador, L. Ouahab, *Eur. J. Inorg. Chem.* **2014**, *2014*, 4558–4563.
[43] X. Yi, K. Bernot, O. Cador, J. Luzon, G. Calvez, C. Daiguebonne, O. Guillou, *Dalton Trans.* **2013**, *42*, 6728–6731.
[44] L. Zhang, J. Jung, P. Zhang, M. Guo, L. Zhao, J. Tang, B. Le Guennic, *Chem. – Eur. J.* **2016**, *22*, 1392–1398.
[45] M. Li, H. Wu, Z. Xia, V. Montigaud, O. Cador, B. L. Guennic, H. Ke, W. Wang, G. Xie, S. Chen, *Chem. Commun.* **2019**, *55*, 14661–14664.
[46] Y. N. Guo, G. F. Xu, W. Wernsdorfer, L. Ungur, Y. Guo, J. Tang, H. J. Zhang, L. F. Chibotaru, A. K. Powell, *J. Am. Chem. Soc.* **2011**, *133*, 11948–11951.
[47] D. Guettas, V. Montigaud, G. F. Garcia, P. Larini, O. Cador, B. Le Guennic, G. Pilet, *Eur. J. Inorg. Chem.* **2018**, 333–339.
[48] D. Guettas, C. M. Balogh, C. Sonneville, Y. Malicet, F. Lepoivre, E. Onal, A. Fateeva, C. Reber, D. Luneau, O. Maury, et al., *Eur. J. Inorg. Chem.* **2016**, *2016*, 3932–3938.
[49] F. Baril-Robert, S. Petit, G. Pilet, G. Chastanet, C. Reber, D. Luneau, *Inorg. Chem.* **2010**, *49*, 10970–10976.
[50] S. Petit, F. Baril-Robert, G. Pilet, C. Reber, D. Luneau, *Dalton Trans.* **2009**, 6809–6815.
[51] H.-R. Tu, W.-B. Sun, H.-F. Li, P. Chen, Y.-M. Tian, W.-Y. Zhang, Y.-Q. Zhang, P.-F. Yan, *Inorg. Chem. Front.* **2017**, *4*, 499–508.
[52] A. Abragam, B. Bleaney, *Electron Paramagnetic Resonance of Transition Ions*, Oxford University Press, Oxford, **2012**.
[53] G. M. Sheldrick, *Acta Crystallogr. Sect. Found. Adv.* **2015**, *71*, 3–8.
[54] G. M. Sheldrick, *Acta Crystallogr. A* **2008**, *64*, 112–122.

Accepted Manuscript

Insert graphic for Table of Contents here.

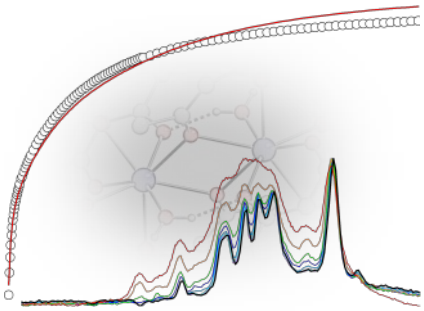

Dysprosium dinuclear complex textbook example is used to marry both magnetism and luminescence in the frame of crystal field theory. This historical theory coupled with Boltzmann population allows the extraction of the energy spectrum of the ground state multiplet from luminescence that is used to model the magnetic properties.

Accepted Manuscript